Near infrared dye-labelled polymeric micro- and nanomaterials: *in vivo* imaging and evaluation of their local persistence

Received 00th January 20xx,
Accepted 00th January 20xx

DOI: 10.1039/x0xx00000x

www.rsc.org/

Gracia Mendoza[a,b†*], Isabel Ortiz de Solorzano[a,b,c†], Inmaculada Pintre[a], Sara Garcia-Salinas[a,b,c], Victor Sebastian[a,b,c], Vanesa Andreu[a,b], Marina Gimeno[d], Manuel Arruebo[a,b,c]

The use of micro- and nanomaterials as carriers of therapeutic molecules can enhance the efficiency of treatments while avoiding side effects thanks to the development of controlled drug delivery systems. The binding of a dye to a drug or to a drug-carrier has opened up a wide range of possibilities for an effective *in vivo* optical tracing of drug biodistribution by using non-invasive real-time technologies prior to their potential use as therapeutic vectors. Here, we describe the fluorescent tagging of polymeric micro- and nanomaterials based on poly(lactic-co-glycolic) acid and on the thermoresponsive poly(N-isopropylacrylamide) with the fluorescent probe IR-820 which was chemically modified for its covalent coupling to the materials. The chemical modification of the dye and the polymers yielded micro- and nanoparticulated labelled-materials to be potentially used as drug depots of different therapeutic molecules. *In vitro* biological studies revealed their reduced cytotoxicity. A spatiotemporal *in vivo* micro- and nanoparticle tracking allowed the evaluation of the materials biodistribution showing their local persistence and high biocompatibility after pathological studies. These results underline the suitability of those materials for the local, sustained, not harmful and/or on-demand drug delivery and the remarkable importance of evaluating materials biodistribution and tissue persistence for their use as local drug depots.

Introduction

To engineer improved drugs and carrier systems for the delivery of therapeutic compounds in the target tissue is one of the main challenges in present biomedicine. Oral absorption or intravenous (IV) drug administration produce a systemic distribution of the drug that can lead to unwanted side effects in non-pathological tissues. The development of site-specific or targeted therapies is closely linked to the profound knowledge of drug biodistribution in order to increase selectivity and decrease unwanted side effects. In this regard, the use of carriers, i.e., micro- and nanoparticles (NPs), has attracted increasing interest thanks to their ability to preserve therapeutic molecules from metabolism and to provide with site-specificity.[1]

In order to deepen into *in vivo* drug biodistribution, the tracking of drug carriers has been widely studied by using radiotracers, obtaining the distribution of the drug carrier by liquid scintillation counting[2] or by scintillating proximity assays based on immune recognition.[3] However, the synthesis and manipulation of radiolabelled materials imply some occupational risks and the required resources are not always affordable; therefore, the search of safer and equally effective technologies represents an ongoing scientific task. Medical imaging encompasses techniques based on different physical or chemical approaches such as ultrasonography, elastography, molecular imaging or chemical shift imaging.[4] Imaging techniques are widely used in diagnosis, progression and treatment of different diseases in the medical field due to their outstanding role in the deeper understanding of *in vivo* molecular events.[5] These techniques are classified in morphological (e.g., magnetic resonance imaging (MRI), computed tomography (CT)) and functional and molecular techniques (e.g., optical imaging, functional magnetic resonance imaging (fMRI), positron emission tomography (PET) and single-photon emission computerized tomography (SPECT)).[6,7] Optical imaging allows the non-invasive real-time imaging of physiological events in living organisms using non-ionizing radiation. It is based on the light emission by bioluminescence, in which takes part the enzyme luciferase and the substrate luciferin, or by fluorescence, that involves the absorption of light at a specific wavelength to emit light at a higher wavelength.[6,8] Bioluminescence relies on the conversion of chemical energy into light and the detection of photons emitted by living cells or tissues though with the requirement of the expression of the enzyme luciferase, whereas fluorescence is supported on light absorption without the involvement of any endogenous molecule.[8] Optical imaging techniques present advantages compared to other techniques, such as safer manipulation, reduced costs and a

[a]*Department of Chemical Engineering. Aragon Institute of Nanoscience (INA), University of Zaragoza, Campus Río Ebro-Edificio I+D, C/ Poeta Mariano Esquillor S/N, 50018-Zaragoza, Spain*
[b]*Aragon Health Research Institute (IIS Aragón), 50009 Zaragoza, Spain*
[c]*Networking Research Centre on Bioengineering, Biomaterials and Nanomedicine, CIBER-BBN, 28029-Madrid, Spain*
[d]*Department of Animal Pathology, University of Zaragoza, C/ Miguel Servet 177, 50013-Zaragoza, Spain*
†*Both authors contributed equally to this work*
**Address correspondence to gmmenc@unizar.es*
Electronic Supplementary Information (ESI) available: supporting material and methods, associated references, one table and five figures. See DOI: 10.1039/x0xx00000x

faster and more reliable response as they are not restricted to anatomical or physiological processes.[5,9,10] Considering these advantages, the optical imaging technique called IVIS (*in vivo* imaging system) has emerged as a useful preclinical method for facilitating the diagnosis in different biomedical fields such as pharmacology, oncology or immunology.[9]

In this regard, the development of safer and novel fluorescent organic dyes has yielded interesting derivatives which combine in the same molecule water solubility (e.g., mediated by functionalization), high quantum yield, reduced photobleaching and stability to enhance the molecule lifetime and to guarantee near infrared (NIR) emission with elevated signal-to-noise ratio.[11, 12] NIR dyes appear as useful tools for fluorescence detection and imaging due to their reduced light scattering and almost no interference regarding tissue autofluorescence.[13-15] Among them, only methylene blue and indocyanine green (ICG) are approved dyes by the Food and Drug Administration (FDA) as extrinsic fluorescent contrast agents.[16] Methylene blue medical uses are much more restricted than ICG, which has been widely used in the evaluation of the hepatic and cardiac function and in ophthalmic angiography.[14, 16-18] However, it has been reported its low stability, slight *in vitro* toxicity (10 µM after 72 h of incubation) and quick liver clearance,[19] pointing to the outstanding necessity of developing novel or even superior NIR dyes for biomedical imaging.

IR-820 is a NIR dye with an improved *in vitro* and *in vivo* stability compared to ICG and the same optical properties.[20] Furthermore, its chemical modification to be anchored to polymers has been shown as a more effective approach than the use of the free fluorophore,[21] highlighting its potential to allow an efficient tracking of *in vivo* drug carrier biodistribution.

The biodegradable and biocompatible properties of polymeric micro- and nanomaterials make them very attractive to tune their lifetime and play an important role in the sustained or triggered release of drugs[22] or even in the photodynamic treatment of cancer.[23-25] Poly(lactic-co-glycolic) acid (PLGA), a building polymer in many FDA-approved biomedical products, has been widely described as nanocarrier protecting NIR dyes from degradation.[26-28] This fact, together with the well-known biocompatibility of PLGA for therapeutic approaches, points to the suitability of these systems for *in vivo* biomedical imaging. In fact, the successful loading of drugs and NIR dyes in PLGA nanosystems has been widely evaluated in *in vivo* tumour models.[29,30] The thermoresponsive polymer polyN-isopropylacrylamide (PNIPAM) shows the possibility to trigger the delivery of a drug in response to temperature changes. The increase in temperature above its lower critical solution temperature (LCST) produces the collapse of the polymer domains and the shrinkage of the particles.[31] Furthermore, the need of long-term therapies in pathologies as diverse as cancer, cardiovascular affections or chronic pain, has produced the compelling development of sustained or triggerable release carriers or scaffolds in order to obtain the required drug release avoiding multiple administrations. These novel carriers based on PLGA and/or PNIPAM have shown release times *in vivo* up to 28 days after local administration, much longer than systemic administrations and preventing the non-specific delivery of drugs and the subsequent side effects.[32-35]

The aim of this work is to develop novel polymeric micro- and nanomaterials of different sizes dye-labelled with the NIR dye IR-820 to track their *in vivo* biodistribution and persistence after intramuscular (IM) and subcutaneous (SC) administration in nude mice. The chemical modification of the dye enabled the covalent attachment to the polymers as terminal groups to obtain stable and biocompatible materials for potential drug delivery applications allowing a simultaneous tracking of the drug carrier. The dye-labelled materials were physico-chemically characterized and *in vitro* tested for their cytotoxicity. *In vivo* studies after IM and SC injection were carried out to test their persistence, biodistribution and tissue response.

Experimental section

Supplementary materials and methods and any associated references are available in the Supplementary Material section.

Synthesis and characterization of PLGA and PNIPAM dye-labelled materials

Carbodiimide covalent labelled PLGA by the amino-modified IR820 (PLGA-IR820-NH_2), PLGA encapsulating the NIR dye (PLGA-IR820 encapsulated) during the NP simple emulsion synthesis, tagged PNIPAM by the acidic-modified IR820 added during the polymer synthesis (PNIPAM-IR820-COOH) or after the NPs synthesis (PNIPAM-IR820-COOH post-synthesis) by covalent carbodiimide bond, labelled PNIPAM microgels by the fluorophore (PNIPAM-IR820 microgels) through contact incubation and tagged PNIPAM microparticles (MPs) by IR820 (PNIPAM-IR820 microparticles) in the same way than microgels were synthesized and characterized as detailed in the Supplementary Material section. Briefly, NPs were synthesized by single emulsion while PNIPAM-IR820 MPs were prepared by microfluidic LED photopolymerization and PNIPAM-IR820 microgels by precipitation polymerization in a batch reactor. Following the synthesis, IR-820 was either encapsulated within PLGA during the emulsion formation to render PLGA-IR820 encapsulated or chemically modified to provide it with reactive functional groups to be bound to the different micro- or nanoparticles. PLGA-IR820-NH_2, PNIPAM-IR820-COOH and PNIPAM-IR820-COOH post-synthesis were fluorescently labelled by using carbodiimide coupling (EDC/NHS) of the modified dye and the corresponding NP. The modified dyes and the materials obtained were further characterized by UV-vis spectroscopy, scanning electron microscopy (SEM), Fourier transform infrared spectroscopy (FTIR), mass spectrometry and NMR spectroscopy. Transmittance studies were also carried out with the PNIPAM modified material in order to confirm the stability of its LCST.

Biological studies

The cytotoxicity of the labelled materials was studied at three essential levels: cell metabolism, cell cycle and endotoxin content.

The studies regarding cell cultures were performed on five different cell lines after treatment for 48 h with the different materials prepared.

Human dermal fibroblasts were obtained from Lonza (Belgium) and THP1 human monocytes from the American Type Culture Collection (ATCC, US). Human tumour cells U251MG and mouse mesenchymal stem cells (mMSCs) were kindly gifted by Dr Pilar Martín-Duque. Fibroblasts and U251MG cells were cultured in DMEM high glucose (Biowest, France) containing 2 mM L-glutamine and supplemented with 10% v/v fetal bovine serum (Gibco, UK) and 1% penicillin-streptomycin-amphotericin B (Biowest, France). Monocytes were grown in RPMI 1640 (Biowest, France) containing 2 mM L-glutamine and supplemented with 10% v/v fetal bovine serum (Gibco, UK), 1% HEPES (Lonza, Belgium), 0.1% 2-mercaptoethanol 50 mM (Gibco, UK), 1% non-essential aminoacids, 1% sodium pyruvate 100 mM and 1% penicillin-streptomycin-amphotericin B (Biowest, France). The *in vitro* differentiation of monocytes to macrophages was performed by the addition of 1 µM phorbol 12-myristate 13-acetate (PMA) (Sigma Aldrich, US) to the cell culture medium for 72 h obtaining the characteristic adherent morphology of macrophages. mMSCs were cultured in DMEM-F12 (Biowest, France) supplemented with 1% glutamine (Gibco, UK), 10% FBS (Gibco, UK) and 1% penicillin-streptomycin-amphotericin B (Biowest, France). All cell types were cultured at 37 ºC and 5% CO_2, except for mMSCs which were grown in hypoxia (3% O_2).

As previously mentioned, the materials tested were PLGA-IR820-NH_2, PLGA-IR820 encapsulated, PNIPAM-IR820-COOH, PNIPAM-IR820-COOH post-synthesis, PNIPAM-IR820 microgels and PNIPAM-IR820 MPs. The cell types described above were incubated with these materials for 48 h to study cell viability and cell cycle.

Blue Cell Viability assay (Abnova) was used to evaluate the viability related to cell metabolism after incubation with the materials (0.1-2 mg/mL) for 48 h. The reagent was added to the cells (10%) and after incubation (4 h, 37 ºC, 5% CO_2), fluorescence was recorded (535/590 nm ex/em) in a Synergy HT Microplate Reader (Biotek, US). Control samples without cells were also run to evaluate a potential NP interference in the assay. Cell viability was calculated by interpolation of the emission data exerted by the treated samples and the control ones (control samples = 100% viability).

The distribution of cell cycle phases was determined by flow cytometry. Cells were exposed for 48 h to materials (1 mg/mL), collected in PBS, fixed in 70% ice-cold ethanol and incubated at 4 ºC for 24 h. Then, DNA was stained by adding a solution of 50 µg/mL propidium iodide and 100 µg/mL RNase A in PBS. DNA content was analysed in a FACSARRAY BD equipment and cell cycle was determined by using the software MODIFIT 3.0 Verity. Negative controls were also run to compare the basal level of cell cycle to that obtained after materials treatment and control samples without cells were also analysed to test a potential NP interference with the methodology.

Endotoxins or lipopolysaccharides (LPS) are bioactive heat-stable molecules present in the outer cell-wall of gram-negative bacteria. They can induce inflammation and immune response of the host organism or even sepsis.[36,37] During the production and handling of micro- and nanomaterials, these materials can be contaminated with endotoxin with the subsequent health risks in a potential future application.[37] Due to this potential concern, we performed the quantification of endotoxin content in our materials prior to their *in vivo* application.

The Endpoint Chromogenic LAL assay (QCL-1000) (Lonza, Belgium) was developed to quantify the endotoxin content in the different materials (1 mg/mL) according to the manufacturer's indications. In brief, 50 µL of diluted samples (1:100 to 1:750 dilution in endotoxin-free water) were dispensed in duplicate in each well of a microplate well. LAL reagent was then added and subsequently the plate was shaken and incubated (37 ºC, 10 min). Following incubation, pre-warmed chromogenic substrate was added and the plate was again incubated (37 ºC, 6 min). Finally, the reaction was stopped (10% SDS solution) and absorbance read at 405 nm in a Synergy HT Microplate Reader (Biotek, US). The determination of the endotoxin levels in the samples was calculated as indicated by the manufacturer.

***In vivo* studies**

All procedures were carried out under Project License 02/16 approved by the Ethic Committee for Animal Experiments from the University of Zaragoza (Spain). The care and use of animals were performed accordingly with the Spanish Policy for Animal Protection RD53/2013, which meets the European Union Directive 2010/63 on the protection of animals used for experimental and other scientific purposes.

Five- to eight-week-old female BALB/c nu/nu mice (Janvier, France) were used for these studies. Mice were anesthetized with 5% isoflurane under oxygen flow of 1 L/min and maintained with a 2%. All animals received subcutaneous (SC; 200 µL) or intramuscular (IM; 20 µL) injections of the materials described above (1 mg/mL) diluted in saline solution (or saline solution in control animals) in order to evaluate the biodistribution and persistence of locally administered injections. Animals were examined daily with especial attention to the injection site.

Our purpose was to target the key tissue avoiding systemic administration and to further investigate the differences between both administrations taking into account the different volumes administered as well as the different metabolic rates of both tissues. Thus, imaging analysis was developed at different time points up to 7 days when using IM administration and 14 days when using SC administration in an IVIS® Lumina Xenogen equipment and Living Image® software (Caliper, US).

In addition, the persistence of IM and SC-administered not labelled PNIPAM MPs in tissue was also assayed in order to elucidate their long-term persistence and the possible damage to tissues after 30 and 60 days p.i. PLGA NPs were not included in this study as it is widely known their tunable persistence depending on its monomeric composition and safety *in vivo*.[33,38] As before, MPs were administered IM and SC at the same conditions stated above and animals were euthanized at 30 and 60 days p.i.

Pathologic studies

All animals were euthanized by cervical dislocation under 5% isoflurane anaesthesia under oxygen flow of 1 L/min (unconsciousness condition). A full post mortem procedure was carried out with special attention to the injection site (subcutaneous tissue, muscular tissue, inguinal and popliteal lymph nodes). These studies were performed to assess the safety and

biocompatibility of the synthetized materials at a local and systemic level, complementing the *in vitro* cell studies. Representative sections of the injection area and local lymph nodes, lung, heart, brain, liver, spleen, kidney and gastrointestinal organs were systematically collected. Tissues were fixed in 4% buffered paraformaldehyde and embedded in paraffin. Five-micron-thick tissue sections were obtained and stained with haematoxylin and eosin (HE). Masson's trichrome staining was applied to skin samples to better describe connective tissue reaction to the materials at the injection area.

Results and discussion

Synthesis and characterization of dye-labelled materials

PLGA and PNIPAM micro- and nanoparticles (MPs and NPs) were labelled with the IR-820 dye through three different methodologies in order to obtain dye-labelled materials of different sizes for potential drug delivery approaches as depot devices: 1) Labelling the polymer prior and after particle formation, 2) Trapping the dye during the particle formation by emulsification and solvent evaporation, 3) Loading the dye after particle formation by diffusion. IR-820 was chemically modified with amine and carboxyl groups to enable a proper labelling of PLGA and PNIPAM and to prevent its detachment from the carrier. The chemically modified IR-820 and the labelled polymers were conveniently studied by NMR spectroscopy of 13C and 1H, Fourier transform infrared spectroscopy (FTIR) and mass spectrometry in order to determine their purity and their chemical and spectral stability (Figures S1-S4).

Comparing the amino- and carboxy-functionalized dyes with plain IR-820 dissolved in methanol we observed that the IR-820 derivatives exhibited a larger Stokes shift (difference between the excitation and emission wavelengths of the same electronic transition) compared to the unmodified IR-820 (Figure S5). This ensures a better performance of the modified dyes since it reduces the chances of self-quenching. Thus the resulting dyes were more sensitive NIR fluorescent probes than the non-functionalized ones. When the solvent was changed to water, the fluorescence decreased for both IR-820 and IR820-COOH (data not shown), in agreement with the previous literature[39] that also reported in cyanine dyes lower values of quantum yield when using water as solvent.

The characterization of modified polymers was carried out in order to evaluate their chemical and spectral properties as NIR fluorophores (Figures S3 and S4). However, in the case of PNIPAM, its thermoresponsive behaviour must be preserved after chemical modification. To ensure it, a transmittance curve of the chemically modified polymer was compared to the non-modified one, observing insignificant variations and exerting a transition temperature of around 36.5 ºC at 50% transmittance for both compounds (data not shown).

The study of the absorbance and fluorescence of the dye-functionalized polymers revealed similar optical performance compared to the not modified dye in terms of Stokes shift and stability. Table 1 summarizes the maximum absorbance and emission values for these polymeric dispersions. PLGA-IR820 could only be measured in acetone because it is not soluble in methanol or water. For that reason, no comparison with the dyes could be exerted, as the dyes are insoluble in acetone. In the case of PNIPAM-IR820, the effect of the solvent is similar increasing the Stokes shift in water, being the value for this polymer the highest of all the measured samples. This fact indicates that the attachment of the dye to the polymer did not alter significantly the emission properties of the dye as its emission range still remained in the NIR region (750-950 nm).

Considering that the NP size is an important factor for *in vivo* studies, we synthetized six different particles with a wide range of sizes in order to determine differences in their behaviour prior carrying out *in vivo* experimentation. IR820 was internalized in the polymeric vectors by two approaches: 1) Tagging the polymer with the dye and 2) Encapsulating the dye in the polymeric matrix. Size, morphology and loading protocol of the different particles used in this study are summarized in Figure 1. NPs based on PLGA-IR820-NH_2, PLGA-IR820 encapsulated, PNIPAM-IR820-COOH and PNIPAM-IR820-COOH post synthesis were produced through a simple emulsion-evaporation method assisted by ultrasound radiation leading to NP sizes between 119 to 560 nm (Figure 1a-d). Nevertheless, in order to study the *in vivo* animal response to larger particles, PNIPAM microgels and MPs were loaded by diffusion with IR-820 after three days contact in a solution of the saturated fluorophore and subsequent purification (see experimental details in the Supplementary Material section). Their sizes were much larger than those displayed by the other materials synthesized, exerting diameters higher than 600 nm in the case of the microgels (Figure 1e) whereas MPs achieved a mean size up to 439 µm (Figure 1f). After synthesis a potential detachment of the dye from the corresponding particles was discarded after evaluating the fluorescence of the supernatants collected by incubating the particles in saline media.

Table 1. Stokes shift of the polymers in different solvents. Data are presented in nm

Sample	Solvent	λ_{max} abs	λ_{max} em	Stokes shift
IR820	Methanol	819	838	19
PLGA-IR820	Acetone	623	767	144
PNIPAM-IR820	Methanol	664	780	116
PNIPAM-IR820	Water	642	792	150

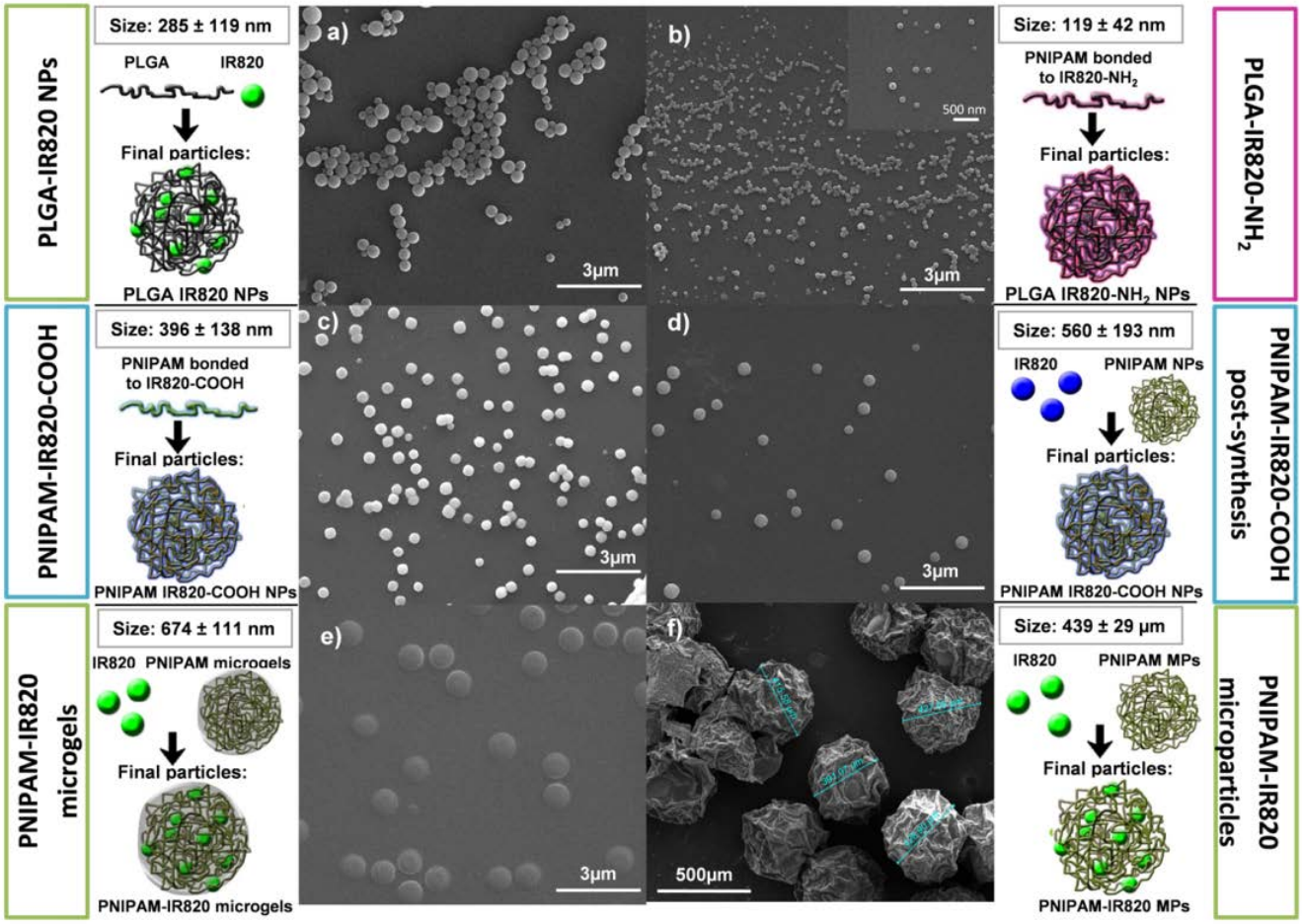

Figure 1 SEM micrographs and loading scheme of the materials synthesized. a) PLGA-IR820 NPs produced by the emulsification-evaporation method. The dye was encapsulated during NPs formation; b) PLGA-IR820-NH_2 produced by the emulsification-evaporation method. The polymer was tagged with the dye prior to NPs formation; c) PNIPAM-IR820-COOH produced by the emulsification-evaporation method. The polymer was tagged with the dye prior to NPs formation; d) PNIPAM-IR820-COOH post synthesis, produced by the emulsification-evaporation method. The polymer was tagged with the dye after NPs formation; e) PNIPAM-IR820 microgels, produced by a polymerization process. The dye was encapsulated after NPs formation; f) PNIPAM-IR820 microparticles, produced by a polymerization-crosslinking process. The dye was encapsulated after NPs formation. Morphology and size of the particles are representative (n ≥ 500; Mean ± SD).

PNIPAM hydrogels tagged with IR820 have been previously developed following the same labelling methodology as ours by submerging hydrogels in an IR-820 solution, though using only one monomer (N-isopropylacrylamide) and reporting a low cloud point (~32 ºC), that is the temperature above which an aqueous solution becomes turbid due to its change in solubility (i.e., coil-to-globule transition), and higher gel sizes (millimetre range), which preclude their biomedical application.[40] Our results clearly show the broad spectrum of sizes of our labelled materials to fulfil different requirements for screening the biodistribution and persistence of different materials widely used as drug delivery vectors. In order to complete the characterization of the different vectors, IR820 concentration was also estimated on each carrier (Table S1) through quantification with the Living Image® software (Caliper, US). A clear correlation between these measured concentrations and the intensity of the *in vivo* signal was not observed, which is consistent with a higher efficiency related to their chemical modification to be anchored to the polymers and their interaction with the surrounding tissues.

In vitro cytotoxicity studies

The cytotoxic effects of the materials described above were analysed on human dermal fibroblasts, monocytes, macrophages, mMSCs and U251MG cells through the treatment of these cell lines with the different synthesized

materials for 48 h. The effects on cell metabolism were assessed by the Blue Cell Viability assay while cell cycle was analysed by flow cytometry. In addition, the endotoxin content of the synthetized materials was also tested to assure their safety for *in vivo* administration. According to the ISO 10993-5 (Biological evaluation of medical devices: Tests for *in vitro* cytotoxicity)[41] a reduction in viability larger than 30% is considered a cytotoxic effect.

The treatment of the cell types assayed with increasing concentrations of PLGA and PNIPAM-IR820-COOH up to 2 mg/mL did not involve a substantial decrease in cell viability in all cases (Figures 2a-c) showing viability percentages higher than 70% at a final concentration of 1 mg/mL. PNIPAM-IR820-COOH post-synthesis (Figure 2d) exerted slightly higher toxic effects on the cell types tested at 2 mg/mL. However, cell viability was higher than 70% at a concentration of 1 mg/mL for macrophages, monocytes and U251MG cells. The effects of cell treatment with PNIPAM-IR820 microgels (Figure 2e) were found more cytotoxic at the highest concentration studied (2 mg/mL) pointing to 1 mg/mL as the non-cytotoxic dose yielding viability percentages higher than 70% on fibroblasts and mMSCs. PNIPAM-IR820 MPs (Figure 2f) showed low cytotoxicity exerting viability percentages higher than 66% at concentrations up to 1 mg/mL.

Furthermore, the viability of mMSCs treated with microgels and MPs was found higher than that obtained for control samples (Figures 2e and 2f). These results may be attributed to the polymeric nature, mechanical features and viscosity of those dispersions, mimicking the extracellular matrix (ECM), and the anchorage dependency of these cells to avoid apoptosis,[42-44] together with the demonstrated higher viability and proliferation of mesenchymal stem cells seeded on PNIPAM gels compared to 2D cultures.[45] Regarding these data,

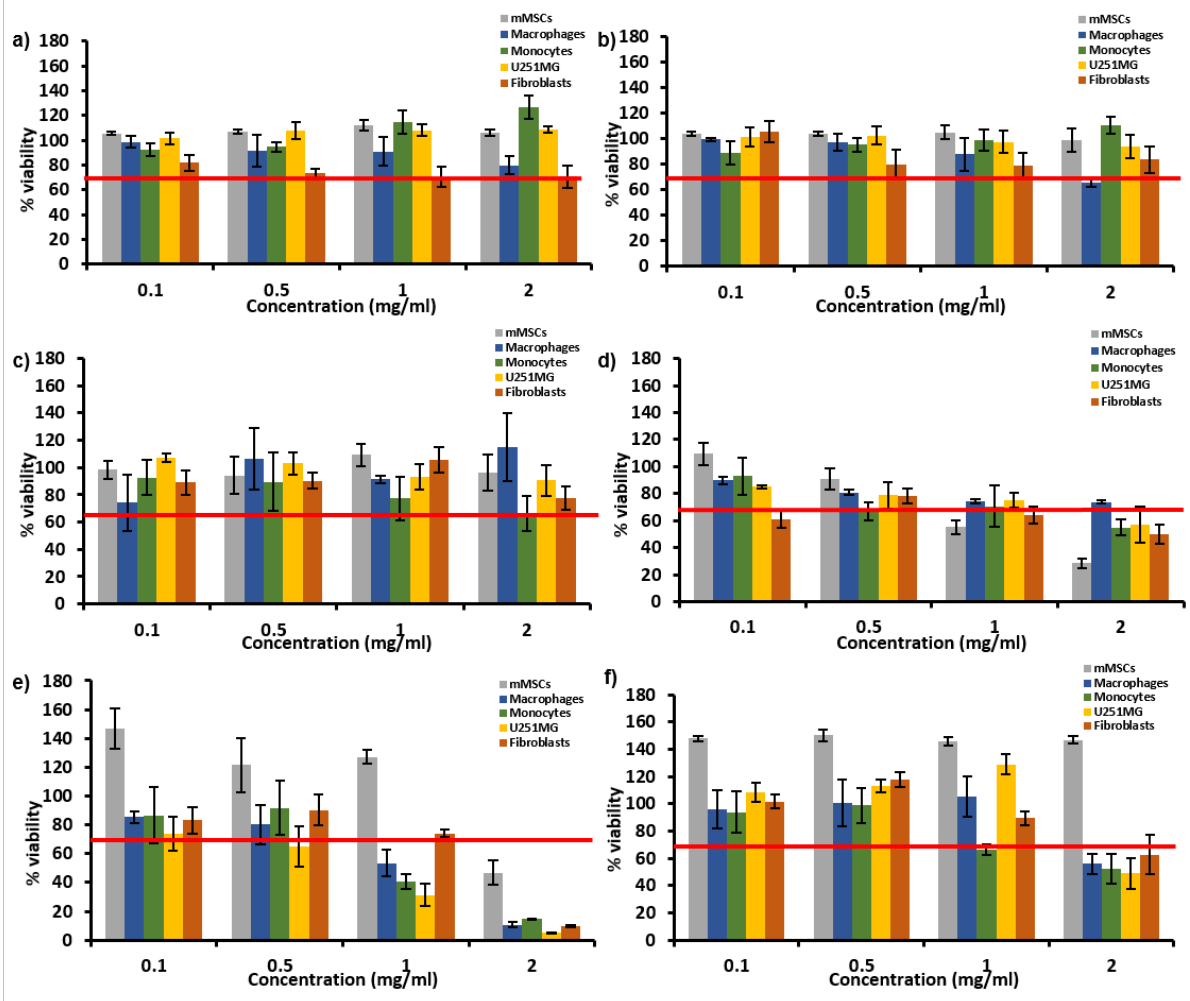

Figure 2 Cell viability of the dye-labelled materials on the five cell lines assayed after 48 h. a) PLGA-IR820 encapsulated; b) PLGA-IR820-NH_2; c) PNIPAM-IR820-COOH; d) PNIPAM-IR820-COOH post synthesis; e) PNIPAM-IR820 microgels; f) PNIPAM-IR820 microparticles. The possible interferences of the labelled materials with the methodology or the reagent were evaluated and discarded. The red mark sets the biocompatilibity threshold percentage (70% viability). Control group (not treated cells) = 100% viability. Data are expressed as Mean ± SD (n = 5).

1 mg/mL was considered as the subcytotoxic concentration for further studies.

The effect of PLGA and PNIPAM at 1mg/mL on cell cycle after 48 h of incubation is shown in Table S2. The addition of PLGA

and PNIPAM at the subcytotoxic dose did not involve an accentuated effect on cell-cycle phase distribution; hence DNA replication and cell division were not affected or halted by these treatments. The addition of PLGA to the cells barely displayed effects on cell cycle, only a slight decrease in G2 phase in U251MG and fibroblasts and a reduced increase in G1 phase in mMSCs were observed.

PNIPAM exerted mild changes in cell-cycle phases being a little more accentuated for PNIPAM-IR820-COOH post-synthesis.

The determination of endotoxin content with the Endpoint Chromogenic LAL assay did not reveal the presence of significant endotoxin concentrations. The measured values were much lower than 0.05 ng/mL (0.5 endotoxin unit (EU)/mL), the safe threshold established by the FDA.[46] In addition, the materials and fluorophores assayed did not show any interference with the reagents or the developed techniques (data not shown).

In conclusion, labelled PLGA and PNIPAM materials did not alter significantly cell metabolism or cell cycle on the cell lines tested at concentrations up to 1 mg/mL, and did not display potentially harmful endotoxin levels for *in vivo* administration, showing their suitability for *in vivo* imaging and potential drug delivery applications.

***In vivo* imaging and biodistribution of dye-labelled materials**

IVIS scanning was used to visualize material biodistribution at different time points after IM and SC administration in nude mice. Figures 3 and 4 displayed the results obtained from these *in vivo* imaging studies. IM administered animals (Figure 3) were visualized until 7 days post-injection (p.i.) while SC administered mice (Figure 4) were analysed until 14 days p.i. IM administration exerted fluorescent signals until the end of the experiments showing the highest intensity when PNIPAM-IR820-COOH post-synthesis was injected while the lowest signals were recorded for dye-labelled PLGA samples at the end of the study. When the materials were SC administered, the intensity of the signal after 14 days p.i. was intense in all mice being superior in both PNIPAM-IR820-COOH samples while the lowest were again displayed by dye-labelled PLGA-treated experimental groups, which may be attributed to the lower proportion of PLGA label susceptible amine functional groups. Furthermore, the signals displayed an increase after 24 h p.i. in SC administrations and also in IM PNIPAM-IR820-COOH post-synthesis and PNIPAM-IR820 microgels due to the well-known binding between the dye and albumin in serum,[47] which probably was also displayed by the other experimental groups though their lower signals hid this increase, and subsequently did not correlate with the dye concentration data explained in Table S1. In addition, at the end of the experiments and immediately after euthanasia, the main organs were *ex vivo* visualized by IVIS scanning to track the possible accumulation of the materials (data not shown) though no trace was observed, highlighting the local biodistribution and persistence of the administered materials. It should be also noted the high intensity of the signal in both types of administrations, pointing to the potential of our labelled materials for the study of micro- and nanoparticle biodistribution as well as for drug delivery taking into account the high biocompatibility of the dye-labelled materials described above.

Pathologic studies

At the necropsy, no animal showed macroscopic lesions compatible with inflammation, infection or degeneration at local or systemic levels. Microscopically, all animals injected with the different synthetized materials (PLGA-IR820 encapsulated, PLGA-IR820-NH_2, PNIPAM-IR820-COOH, PNIPAM-IR820-COOH post synthesis, PNIPAM-IR820 microgels and PNIPAM-IR820 microparticles) did not present any lesions at epidermis, dermis, subcutaneous tissue, musculature or local lymph nodes for both SC and IM administrations (Figure 5).

The group administered with non-labelled PNIPAM MPs used to test the persistence of MPs in tissue, showed foreign body reaction at the subcutaneous musculature at day 60 (Figure 6). This reaction was well circumscribed characterized by active fibroblasts forming a fibrous encapsulation of the eosinophilic amorphous material intermixed with moderate number of macrophages, foreign body giant cells and scarce neutrophils. The collagenous tissue and fibroblast encapsulation of the material was more evident using Masson's trichrome stain. The popliteal lymph node showed a moderate paracortical lymphocyte hyperplasia identified by increased lymphocyte density accompanied by increased paracortical area. No microscopic lesions were found in all remaining organs studied (brain, heart, kidney, liver, lung, spleen and gastrointestinal organs), denoting the lack of systemic toxicity by the synthetized materials.

Drug site-specific biodistribution has become a main issue for the improvement of novel therapeutic strategies and a key aspect to efficiently engineer drug-delivery vectors. The imaging tracking of drug-carrier biodistribution is very relevant to identify the penetration and persistence of the carried drug in treated tissue avoiding biopsy.[48,49] Furthermore, the development of new approaches to improve long-term therapies has entailed the use of sustained or controlled release nanocarriers, which are able to effectively

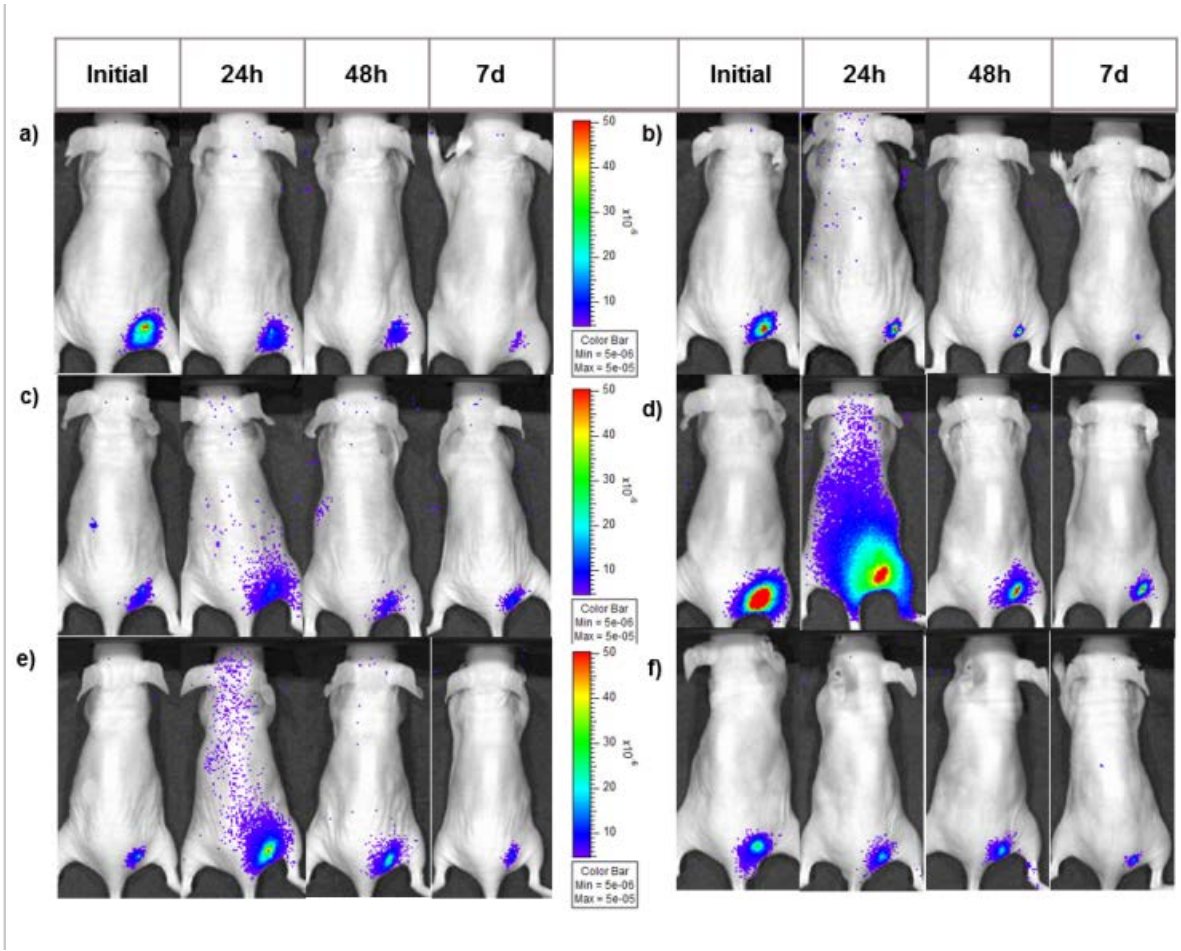

Figure 3 *In vivo* time course fluorescence imaging of labelled materials after intramuscular injection. All signals are presented according to the same color scale. a) PLGA-IR820 encapsulated; b) PLGA-IR820-NH_2; c) PNIPAM-IR820-COOH; d) PNIPAM-IR820-COOH post synthesis; e) PNIPAM-IR820 microgels; f) PNIPAM-IR820 microparticles.

administer the therapeutic dose circumventing recurrent administrations and side effects. Local and targeted delivery of encapsulated drugs mediated by micro- and nanomaterials may increase stability and decrease clearance leading to safer and improved biomedical outcomes. The labelling of these engineered materials to successfully determine their biodistribution is an important step for the deeper knowledge of their behaviour and potential effects. In this study, we have proposed a successfully labelling of polymeric micro- and nanomaterials based on PLGA and PNIPAM with the NIR dye IR-820. Both the fluorescent probe and the polymers were modified in order to show that widely used polymeric materials of different sizes could be labelled for an efficient tracking *in vivo*. Local administration of drugs was developed to improve the efficacy of a drug being placed directly in the target tissue, and consequently reducing potentially harmful side effects. The high biocompatibility and the long tracing of drug-carrying materials highlight the potential of these dye-labelled materials for the safe and controlled delivery of drugs avoiding the direct labelling of drugs since unwanted chemical modifications of the drug could be produced impairing its activity.

Previous studies have shown the formulation of NPs of D-luciferin and NPs of DiR together with D-luciferin for *in vivo* tracking of NPs in tumour treatment.[6] These lipid-based materials showed particle sizes lower than 200 nm and allowed the visualization of tumours more than 24 h, providing long-term tumours visualization though significantly lower than the time points revealed in our studies in which IM and

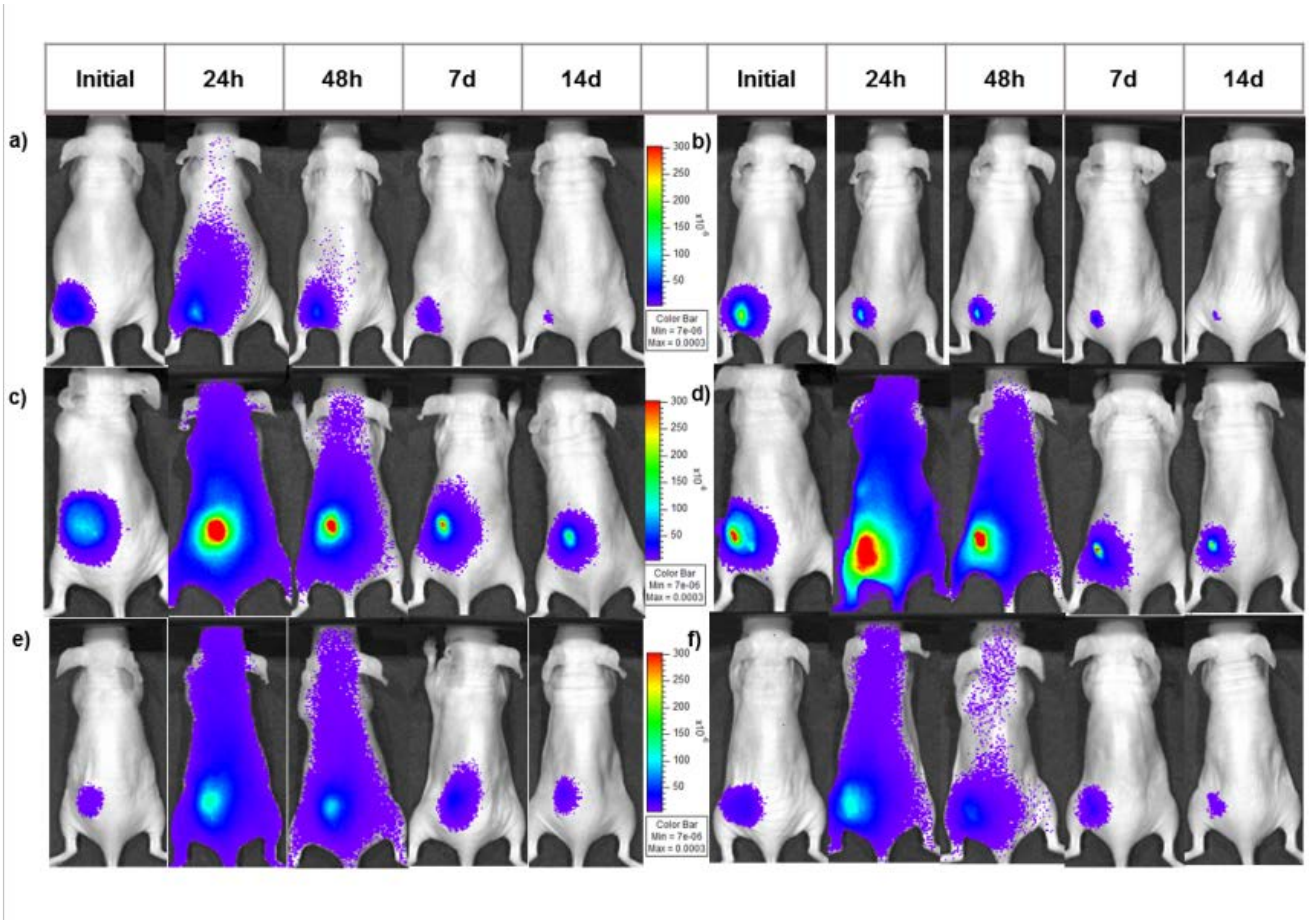

Figure 4 *In vivo* time course fluorescence imaging of labelled materials after subcutaneous injection. All signals are presented according to the same color scale. a) PLGA-IR820 encapsulated; b) PLGA-IR820-NH_2; c) PNIPAM-IR820-COOH; d) PNIPAM-IR820-COOH post synthesis; e) PNIPAM-IR820 microgels; f) PNIPAM-IR820 microparticles.

SC administration displayed fluorescent signals after 7 and 14 days, respectively (Figures 3 and 4).

Other materials have also been labelled for bioimaging and biomedical applications, such as silica NPs[50,51] or calcium phosphate NPs.[52] Silica NPs bearing rhodamine B isothiocyanate (20 or 100 nm), positively or negatively charged to elude the dissociation of the tracer, were orally administered to mice and fluorescence recorded *in vivo* up to 6 h[50]. These studies highlighted the same *in vivo* behaviour of both charged NP types in spite of showing different sizes. Their systemic administration produced an accumulation in lung, kidney and liver, which is not advisable for therapeutic strategies in which more site-specific and efficient vectors and administrations are strongly encouraged. In this regard, other silica modified NPs (20-25 nm) were also covalently NIR labelled and tracked in a mice *in vivo* model after IV administration showing fluorescence signal until the end of the experiments (15 days p.i.), although recording again NP accumulation in the liver.[51] Calcium phosphate NPs were loaded with silk sericin for the development of a new antitumor approach.[52] Then, they were labelled with the NIR dye DiR by post-synthesis addition in order to track their biodistribution in a tumour mice model in which those dye-labelled NPs were administered intravenously. The biodistribution was tracked by IVIS showing that NPs were mostly found in the liver and most of them were also degraded within two weeks. Furthermore, only a low percentage of NPs were localized in the tumour site, pointing to the need of more targeted and safer therapeutic strategies as we propose here.

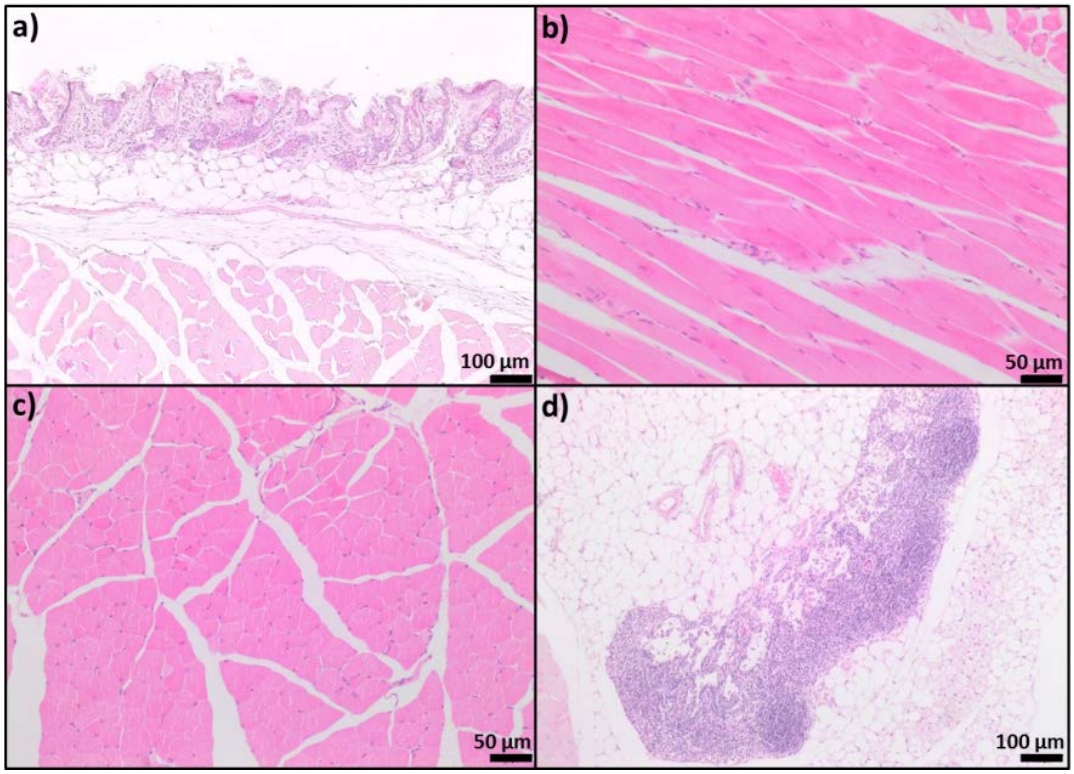

Figure 5 Histological analysis after 7 days (IM) and 14 days (SC) post-injection. a) PNIPAM-IR820 MPs SC injection. Normal histologic features at epidermis, dermis, subcutaneous tissue and musculature, HE 10x; b) PNIPAM-IR820-COOH post-synthesis IM injection. Subcutaneous musculature (longitudinal section). No inflammatory infiltrate is observed between the muscle fibres, myocytes nuclei are well positioned and the fibres aligned, HE 20x; c) PLGA-IR820 encapsulated IM injection. Subcutaneous musculature (cross section). No degeneration or inflammatory lesions at the muscle fibres were observed, HE 20x; d) PNIPAM-IR820 microgels SC injection. Popliteal lymph node. Note preservation of the ratio cortical/medullary thickness, HE 10x.

Liposomes (~200 nm) encapsulating a NIR dye (XenoFluor™-680) and conjugated with a collagen antibody have been successfully tested in the early diagnosis of osteoarthritis in a murine *in vivo* model, achieving the visualization of affected joints by IVIS.[53] However, the presence of those liposomes in other tissues different than knee cartilage was shown in spite of the retro-orbital administration. The esterification of PLGA to obtain polymers modified with nanocrystals has also been developed with diagnostic purposes.[54] Gold nanocrystals and quantum dots were added to the polymer to yield diagnostically active lipid-PLGA NPs (~100 nm), which were detected in an *in vitro* model of mouse macrophages by IVIS though their biocompatibility or their efficiency *in vivo* were not disclosed.

PLGA has been widely used as nanocarrier or depot thanks to its high biocompatibility as it is degraded by simple hydrolysis of its ester bond into acidic monomers, facilitating its elimination from the organism through the endogenous metabolic pathways. However, its persistence in tissue has been recorded at long time points showing its presence after 28 days post-implantation of PLGA scaffolds in a mice model.[33] These studies showed the decrease in the PLGA molecular weight to almost the half of the original one by the end of the experiments and recorded lower cell mobilization and angiogenesis than poly ε-caprolactone-based scaffolds, sustaining the unfavourable environment generated by the acidic monomers released during PLGA degradation, which was not observed in our studies as no harmful tissue reaction was observed even though at shorter time points. In this regard, PLGA-derived depots were fabricated as insulin reservoirs and SC administered in a diabetic murine model[55] or as different therapeutic drug depots IM injected to rabbits[56]

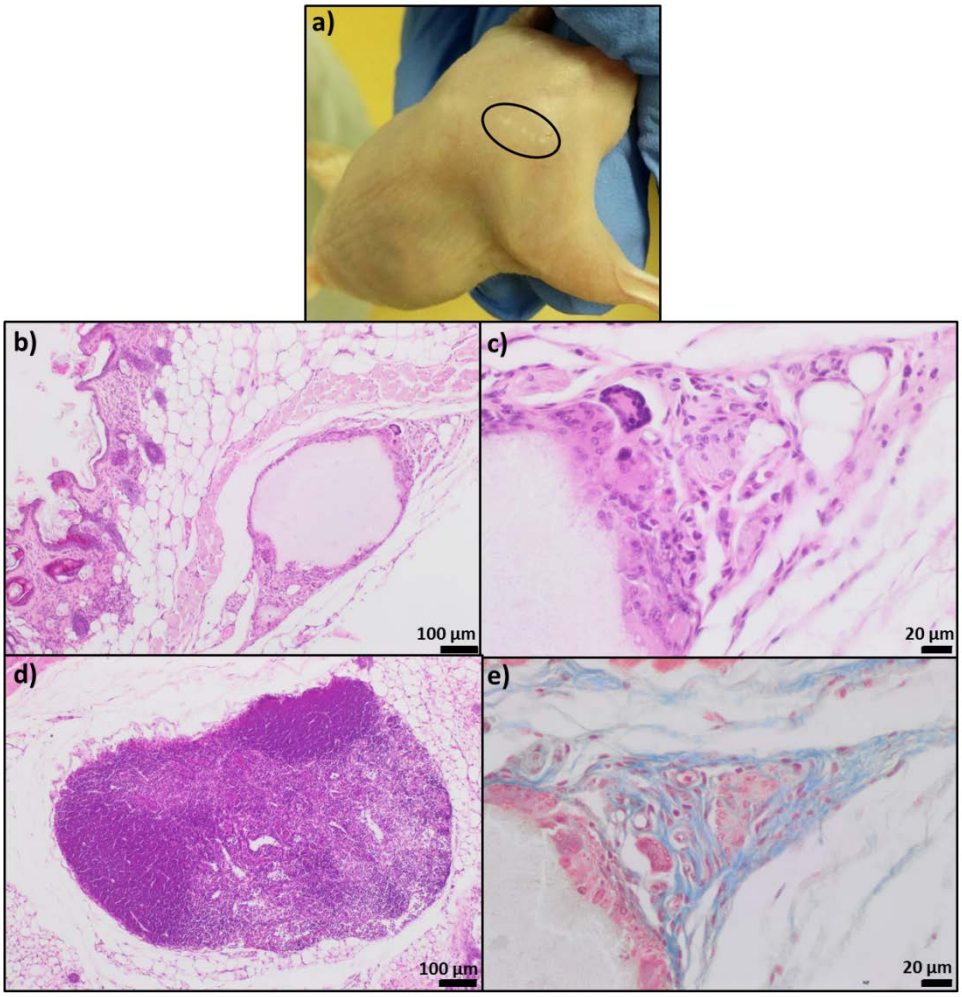

Figure 6 Histological study of the persistence of not-labelled PNIPAM MPs in tissue after injection. a) Macroscopic image of a BALB/c nu/nu mouse. Note the white foreign material (circle) located at the left hindlimb consistent with PNIPAM MPs; b) Well-circumscribed fibrous encapsulation of foreign material at subcutaneous musculature. Moderate amount of fibroblasts and macrophages surrounding the eosinophilic amorphous material, HE 10x; c) Foreign body reaction is manly formed by foamy macrophages, giant cells and spindle-shaped active fibroblasts, HE 40x; d) The number of lymphocytes is increased expanding in the paracortical area. Lymphocytes are mature, small, normal in appearance and within their respective compartments characteristic of lymphoid hyperplasia, HE 10x; e) Blue staining indicating fibroplasia phenomena with formation of collagen fibres surrounding the foreign material, Masson's trichrome stain 40x.

and rats[57], achieving a sustained release up to 16 days, highlighting their suitability as long-term effective reservoirs. In addition, the local delivery of PLGA NPs (~150-170 nm) labelled with coumarin-6 for IVIS imaging was tested in an intravaginal mice model in order to study the feasibility of these nanomaterials for intravaginal and local drug delivery.[58] Their efficiency as imaging vector was shown though only for 24 h after administration and their potential delivery was higher when they were functionalized with PEG or avidin palmitate, due to their lower leakage related to their penetrability and adhesion to tissue mucus. In this sense, NIR labelled (DY-675 and DY-700) PLGA NPs (~200 nm) were imaged after IV injection in murine models.[59,60] Their efficiency was shown, even when only 1% of the labelled polymer was used to prepare the tagged NPs,[60] but biodistribution was only acquired for short periods of time (≤ 24h) and NP accumulation in lungs and/or liver was registered, so their suitability for long term tracing and biomedical applications was not clearly confirmed. Furthermore, PLGA and PLGA-PLA:PEG (poly(lactide)-poly(ethilene glycol)) nanospheres were

SC administered in an *in vivo* rat model in order to test the behaviour and biodistribution of tuned NP surfaces to increase their lymphatic drainage.[61] Blood NP levels and histology up to 24 h p.i. showed an elevated uptake of coated NPs by lymph nodes, which is not in accordance with our studies as their mean sizes were lower than 100 nm in contrast with ours (>100 nm). However, to achieve the sustained drug release for long term or even chronic treatments, this strategy does not seem adequate due to the short lifetime of the polymers in the administration site. To sum up, the use of highly biocompatible polymers ensures the safe administration of therapeutic drugs, achieving long persistence as microparticulated vectors and thus, prolonged drug release rates by acting as depots. These observations point to the greater importance of the biocompatibility of the polymer than the size of the material used.

To the best of our knowledge, this is the first time that IR-820 is anchored to or loaded into PNIPAM and PLGA to obtain a wide range of polymeric material sizes to be tracked in different biomedical strategies. Their biocompatibility and *in vivo* efficiency highlighted their potential benefits compared to radiotracers. Furthermore, PNIPAM lifetime *in vivo* has been also successfully reported without obtaining tissue damage after 60 days. Our promising results point to the suitability of the labelled materials for long-term local and sustained drug delivery or even for the on-demand drug delivery regarding the thermoresponsive ability of PNIPAM, avoiding systemic distribution and tissue damage.

Conclusions

Our study deals with the development and *in vivo* evaluation of labelled biocompatible micro- and nanomaterials for the study of their biodistribution and persistence. The synthesized dye-labelled materials were optimized for biomedical applications with the purpose of their use as drug depots for local affections. The chemical modification of IR-820 to introduce a short linker chain with a terminal carboxylic group or with an amine was successfully carried out. These derivatives showed improved fluorescent properties compared to the unmodified free dye. The acid and amino derivatives of IR-820 prepared allowed the labelling of amino and acid terminated polymers respectively, used later for NP synthesis. IR820-COOH also allowed the labelling of already prepared PNIPAM NPs in a post-grafting reaction.

In vitro studies highlighted their biocompatibility after the evaluation of their effects on different cell lines regarding cell metabolism and cell cycle as well as their endotoxin-free nature. Fluorescent labelled PLGA and PNIPAM expressed local detectable signals up to the end of the studies after 7 days (IM) and 14 days (SC) of the administration exerting higher signals for PNIPAM derivatives due to their higher proportion of label susceptible amine functional groups, pointing to their suitability to study the biodistribution of novel materials intended for medical purposes.

Furthermore, the labelled materials did not show any inflammatory or degenerative process and no lymphadenopathies were observed either. PNIPAM MPs exerted a long-term persistence in tissues after 60 days without showing remarkable harmful effects. These results clearly pinpoint to the potential use of our novel labelled micro- and nanomaterials for the safe and localized drug delivery as well as to the suitability of PNIPAM as a long-term drug carrier. The determination of drugs in physiological fluids (blood, urine, etc.) or in tissues can be challenging and, for that reason, tracking their encapsulating carriers might help when explaining the medical outcome of the drug treatment without the need of drug radiolabeling or using time-consuming chromatographic methods.

Conflicts of interest

There are no conflicts to declare.

Acknowledgements

The authors gratefully acknowledge the financial support of the ERC Consolidator Grant program (ERC-2013-CoG-614715, NANOHEDONISM). CIBER-BBN is an initiative funded by the VI National R&D&i Plan 2008–2011, Iniciativa Ingenio 2010, Consolider Program, CIBER Actions and financed by the Instituto de Salud Carlos III (Spain) with assistance from the European Regional Development Fund. We acknowledge the LMA-INA and Cell Culture, Animal Care, Pathological Anatomy and Medical Imaging and Phenotyping Core Units from University of Zaragoza and IACS/IIS Aragon for their instruments and expertise. The authors declare that they have no conflict of interest.

References

1 R. Korsmeyer, Regen. Biomater., 2016, 3, 143–147.
2 A. Gaudin, S. Lepetre-Mouelhi, J. Mougin, M. Parrod, G. Pieters, S. Garcia-Argote, O. Loreau, J. Goncalves, H. Chacun, Y. Courbebaisse, P. Clayette, D. Desmaële, B. Rousseau, K. Andrieux and P. Couvreur, J. Control. Release, 2015, 212, 50–58.
3 E. R. Gardner, in Handbook of Anticancer Pharmacokinetics and Pharmacodynamics, ed. H. L. Rudek, M. A.; Chau, C. H.; Figg, W. D.; McLeod, Springer New York, New York, 2nd edn., 2014, pp. 107–116.
4 A. M. Lăpădat, I. R. Jianu, B. S. Ungureanu, L. M. Florescu, D. I. Gheonea, S. Sovaila and I. A. Gheonea, J. Med. Life, 10, 19–26.
5 H. Chen and S. H. Thorne, Curr. Protoc. Cytom., 2012, 59, 12.24.1-12.24.11.
6 A. R. Patel, E. Lim, K. P. Francis and M. Singh, Pharm. Res., 2014, 31, 3073–84.
7 J. K. Willmann, N. van Bruggen, L. M. Dinkelborg and S. S. Gambhir, Nat. Rev. Drug Discov., 2008, 7, 591–607.
8 C. E. Badr and B. A. Tannous, Trends Biotechnol., 2011, 29, 624–633.
9 A. C. Freise and A. M. Wu, Mol. Immunol., 2015, 67, 142–52.

10 B. Lim, Y. Yao, A. L.-I. Huang, M. L. Yap, U. Flierl, J. Palasubramaniam, M. T. K. Zaldivia, X. Wang and K. Peter, Theranostics, 2017, 7, 1047–1061.
11 M. Ptaszek, in Progress in molecular biology and translational science, 2013, vol. 113, pp. 59–108.
12 M. Sun, K. Müllen and M. Yin, Chem. Soc. Rev., 2016, 45, 1513-1528.
13 J. O. Escobedo, O. Rusin, S. Lim and R. M. Strongin, Curr. Opin. Chem. Biol., 2010, 14, 64–70.
14 S. L. Gibbs, Quant. Imaging Med. Surg., 2012, 2, 177.
15 Y. Yang, C. Yue, Y. Han, W. Zhang, A. He, C. Zhang, T. Yin, Q. Zhang, J. Zhang, Y. Yang, J. Ni, J. Sun and D. Cui, Adv. Funct. Mater., 2016, 26, 8735-8745.
16 Q. T. Nguyen and R. Y. Tsien, 2013.
17 M. Chen and M. Yin, Prog. Polym. Sci., 2014, 39, 365-395.
18 FDA, Indocyanine Green for Injection, USP, 2006.
19 J. Pauli, T. Vag, R. Haag, M. Spieles, M. Wenzel, W. A. Kaiser, U. Resch-Genger and I. Hilger, Eur. J. Med. Chem., 2009, 44, 3496–3503.
20 A. Fernandez-Fernandez, R. Manchanda, T. Lei, D. A. Carvajal, Y. Tang, S. Z. R. Kazmi and A. J. McGoron, Mol. Imaging, 2012, 11, 99–113.
21 A. Fernandez-Fernandez, R. Manchanda, D. Carvajal, T. Lei, S. Srinivasan and A. McGoron, Int. J. Nanomedicine, 2014, 9, 4631.
22 M. Chen and M. Yin, Prog. Polym. Sci., 2014, 39, 365–395.
23 W. Hou, F. Xia, C. S. Alves, X. Qian, Y. Yang and D. Cui, ACS Appl. Mater. Interfaces, 2016, 8, 1447-1457.
24 C. Yue, C. Zhang, G. Alfranca, Y. Yang, X. Jiang, Y. Yang, F. Pan, J. M. de la Fuente and D. Cui, Theranostics, 2016, 6, 456-469.
25 S. Zhang, W. Guo, J. Wei, C. Li, X. J. Liang and M. Yin, ACS Nano, 2017, 11, 3797-3805.
26 E. P. Porcu, A. Salis, E. Gavini, G. Rassu, M. Maestri and P. Giunchedi, Biotechnol. Adv., 2016, 34, 768–789.
27 V. Saxena, M. Sadoqi, S. Kumar and J. Shao, ed. A. N. Cartwright, International Society for Optics and Photonics, 2004, p. 29.
28 V. Saxena, M. Sadoqi and J. Shao, Int. J. Pharm., 2006, 308, 200–204.
29 R. Manchanda, A. Fernandez-Fernandez, A. Nagesetti and A. J. McGoron, Colloids Surfaces B Biointerfaces, 2010, 75, 260–267.
30 S. Srinivasan, R. Manchanda, T. Lei, A. Nagesetti, A. Fernandez-Fernandez and A. J. McGoron, J. Photochem. Photobiol. B Biol., 2014, 136, 81–90.
31 B. P. Timko, M. Arruebo, S. A. Shankarappa, J. B. McAlvin, O. S. Okonkwo, B. Mizrahi, C. F. Stefanescu, L. Gomez, J. Zhu, A. Zhu, J. Santamaria, R. Langer and D. S. Kohane, Proc Natl Acad Sci U S A., 2014, 111, 1349-1454.
32 B. P. Timko, T. Dvir and D. S. Kohane, Adv. Mater., 2010, 22, 4925–4943.
33 H.-J. Sung, C. Meredith, C. Johnson and Z. S. Galis, Biomaterials, 2004, 25, 5735–42.
34 Z. Ge and S. Liu, Chem. Soc. Rev. Chem. Soc. Rev, 2013, 42, 7289–7325.
35 P. Cheng, W. Zeng, L. Li, D. Huo, L. Zeng, J. Tan, J. Zhou, J. Sun, G. Liu, Y. Li, G. Guan, Y. Wang, C. Zhu, P. Cheng, W. Zeng, L. Li, D. Huo, L. Zeng, J. Tan, J. Zhou, J. Sun, G. Liu, Y. Li, G. Guan, Y. Wang and C. Zhu, .
36 J. C. Hurley, Clin. Microbiol. Rev., 1995, 8, 268–92.
37 S. Smulders, J.-P. Kaiser, S. Zuin, K. L. Van Landuyt, L. Golanski, J. Vanoirbeek, P. Wick and P. H. Hoet, Part. Fibre Toxicol., 2012, 9, 41.
38 A. K. Mohammad and J. J. Reineke, Mol. Pharm., 2013, 10, 2183–2189.
39 X. Peng, F. Song, E. Lu, Y. Wang, W. Zhou, J. Fan and Y. Gao, J. Am. Chem. Soc., 2005, 127, 4170–4171.
40 J. Gregory, M. S. Riasi, J. Cannell, H. Arora, L. Yeghiazarian and V. Nistor, J. Appl. Polym. Sci., 2014, 131, n/a-n/a.
41 ISO 10993-5:2009 - Biological evaluation of medical devices -- Part 5: Tests for in vitro cytotoxicity. http://www.iso.org/iso/catalogue_detail.htm?csnumber=36406.
42 M. Guvendiren and J. A. Burdick, Curr. Opin. Biotechnol., 2013, 24, 841–846.
43 S. S. Ho, K. C. Murphy, B. Y. K. Binder, C. B. Vissers and J. K. Leach, Stem Cells Transl. Med., 2016, 5, 773–81.
44 P. Chiarugi and E. Giannoni, Biochem. Pharmacol., 2008, 76, 1352–1364.
45 L. Yang, F. Cheng, T. Liu, J. R. Lu, K. Song, L. Jiang, S. Wu and W. Guo, Biomed. Mater., 2012, 7, 35003.
46 F. and D. Administration, 1985, 40.
47 S. I. Prajapati, C. O. Martinez, A. N. Bahadur, I. Q. Wu, W. Zheng, J. D. Lechleiter, L. M. McManus, G. B. Chisholm, J. E. Michalek, P. K. Shireman and C. Keller, Mol. Imaging, 2009, 8, 45–54.
48 M. S. Berridge, D. L. Heald and Z. Lee, Drug Dev. Res., 2003, 59, 208–226.
49 B. K. Leong, J. K. Coombs, C. P. Sabaitis, D. A. Rop and C. S. Aaron, J. Appl. Toxicol., 18, 149–60.
50 C.-M. Lee, T. K. Lee, D.-I. Kim, Y.-R. Kim, M.-K. Kim, H.-J. Jeong, M.-H. Sohn, S. T. Lim and S. T. Lim, Int. J. Nanomedicine, 2014, 9 Suppl 2, 243–50.
51 R. Kumar, I. Roy, T. Y. Ohulchanskky, L. A. Vathy, E. J. Bergey, M. Sajjad and P. N. Prasad, ACS Nano, 2010, 4, 699–708.
52 R. Zhao, X. Ren, C. Xie and X. Kong, Microsc. Res. Tech., 2017, 80, 321–330.
53 H. Cho, E. Pinkhassik, V. David, J. M. Stuart and K. A. Hasty, Nanomedicine Nanotechnology, Biol. Med., 2015, 11, 939–946.
54 A. J. Mieszawska, A. Gianella, D. P. Cormode, Y. Zhao, A. Meijerink, R. Langer, O. C. Farokhzad, Z. A. Fayad and W. J. M. Mulder, Chem. Commun. (Camb)., 2012, 48, 5835–7.
55 B. Jeong, K. M. . Lee, A. Gutowska and Y. H. An, 2002.
56 T. A. Ahmed, Y. A. Alharby, A.-R. M. El-Helw, K. M. Hosny and K. M. El-Say, Drug Des. Devel. Ther., 2016, 10, 405–15.
57 G. V. Shavi, U. Y. Nayak, M. S. Reddy, K. Ginjupalli, P. B. Deshpande, R. K. Averineni, N. Udupa, S. S. Sadhu, C. Danilenkoff and R. Raghavendra, Mater. Sci. Eng. C, 2017, 75, 535–544.
58 Y. Cu, C. J. Booth and W. M. Saltzman, J. Control. Release, 2011, 156, 258–64.
59 G. Tosi, L. Bondioli, B. Ruozi, L. Badiali, G. M. Severini, S. Biffi, A. De Vita, B. Bortot, D. Dolcetta, F. Forni and M. A. Vandelli, J. Neural Transm., 2011, 118, 145–153.

60 R. Reul, N. Tsapis, H. Hillaireau, L. Sancey, S. Mura, M. Recher, J. Nicolas, J.-L. Coll, E. Fattal, C. Vauthier, E. Fattal, B. Gillet, W. Urbach, S. L. Bridal and E. Fattal, Polym. Chem., 2012, 3, 694.
61 A. E. Hawley, L. Illum and S. S. Davis, Pharm. Res., 1997, 14, 657–661.